Robust Wave Equation Migration Velocity Analysis Using a Normalized Differential Semblance Misfit Function

Abdullah Alali, Bingbing Sun, Tariq Alkalifah

March 9, 2020

Summary

The wave equation migration velocity analysis (WEMVA) techniques try to estimate an accurate subsurface velocity model for migration purposes by relying on the full-wave equation. A popular method in WEMVA is the differential semblance optimization (DSO). The objective function of DSO applies a penalty operator to extended subsurface images to minimize the energy residing in the non-physical extension. The penalty operator used in conventional DSO actually tries to reduce the energy instead of focussing it toward the subsurface zero offset. We introduce a normalization term to the DSO method in which we use a pseudo inverse Born operator to calculate the extended image and show that the new objective is more efficient and robust in focusing the energy and eliminating artifacts in the process of estimating the macro-velocity model.

Introduction

Differential semblance optimization (DSO) is the most popular method in the wave equation migration velocity analysis (WEMVA) (Sun and Alkhalifah, 2018b). It is performed by extending the image in extra space (Rickett and Sava, 2002) and applying an annihilator to penalize the energy in these non-physical extensions (Symes, 2008).

The conventional penalty-function based DSO method tries to reduce the energy in the subsurface offset gathers rather than focus it toward zero offset. This undesirable behavior would hamper the inversion process with slower convergence and unstable update. In this abstract, we propose to modify the penalty function in DSO with an additional normalization term. A similar misfit function has been used and analyzed in full waveform inversion (Warner and Guasch, 2016; Sun and Alkhalifah, 2018a,c, 2019), we extend its application in image domain MVA here.

In this abstract, a pseudo inverse (Chauris and Cocher, 2017) is adopted to implement the normalized DSO misfit function, and we use a two-layer model and Marmousi model to demonstrate the good performance of the proposed method.

Theory

The conventional DSO misfit function takes the form,

$$J_{\text{DSO}} = \frac{1}{2}\big|\big|\, hI(\mathbf{x},h)\big|\big|_2^2, \tag{1}$$

where $\mathbf{x} = (x,z)$ is the coordinates in 2D and h is the subsurface offset. The extended image $I(x,h)$ is obtained using a pseudo inverse formula (Chauris and Cocher, 2017) that reads,

$$\begin{aligned} I(\mathbf{x},h) = &\frac{32}{v_{0+}v_{0-}} D_z \int \frac{\tilde{\Omega}(\omega)}{i\omega} D_{s_z} S(\mathbf{x}_s, \mathbf{x}-h, \omega) \\ &D_{r_z} R(\mathbf{x}+h, \mathbf{x}_r, \omega)\, d\omega\, d\mathbf{x}_s\, d\mathbf{x}_r, \end{aligned} \tag{2}$$

where $v_{0+} = v(x+h)$ and $v_{0-} = v(x-h)$ are shifted background velocities. $\tilde{\Omega}(\omega)$ is the inverse of the source wavelet. D_{r_z} and D_{s_z} are derivatives with respect to the vertical dimension of the receiver and source positions, respectively. S and R are the source and the receiver wavefields, respectively.

The normalized differential semblance (NDSO) misfit function is formulated by adding a normalization term $||I(\mathbf{x},h)||_2^2$ to equation (1)

$$J_{\text{NDSO}} = \frac{1}{2}\frac{\big|\big|\, hI(\mathbf{x},h)\big|\big|_2^2}{\big|\big|I(\mathbf{x},h)\big|\big|_2^2}. \tag{3}$$

The gradient for both objectives is given by,

$$\frac{\partial J}{\partial v} = \frac{\partial I}{\partial v}^* \frac{\partial J}{\partial I}. \tag{4}$$

For conventional DSO,

$$\frac{\partial J_{DSO}}{\partial I} = h^2\, I(\mathbf{x},h), \tag{5}$$

while for NDSO,

$$\frac{\partial J_{NDSO}}{\partial I} = \frac{(h^2 - 2\,J)\;\; I(\mathbf{x},h)}{\big|\big|\, I(\mathbf{x},h)\big|\big|_2^2}. \tag{6}$$

The term $\frac{\partial I}{\partial v}$ is the derivative of the subsurface offset image with respect to the velocity. The total gradient calculation is often derived using the adjoint-state method and can be found in Plessix (2006) and Lameloise et al. (2015).

Figure 1(a) shows the energy distribution for the subsurface offset image when the velocity model is incorrect. In this case, the energy is spread out along the offset axis. Our inversion target is to try to focus the energy in the offset gather toward the zero offset as shown in Figure 1(c). However, as shown in Figure 1(b) the conventional DSO misfit function may reduce the amplitude at all offsets rather than focus it toward the zero offset. For example, if $I(x,h)$ evolves to $\lambda I(x,h)$ where $\lambda < 1$, the DSO function of equation (1) shows reduced value although $\lambda I(x,h)$ do not show any focusing behavior compared to $I(x,h)$. The NDSO misfit function in equation (3) do not have those issues as the added normalization term would force the image gather to focus and reducing the amplitude at all offsets would have limited effect in the resulting misfit value. As a result, $I(x,h)$ and $\lambda I(x,h)$ would have the same J_{NDSO} values, even if λ is extremely small.

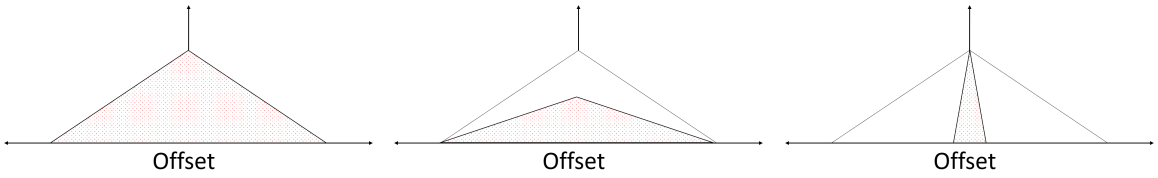

(a) (b) (c)

Figure 1 *A schematic describing the energy distribution (a) in the case of an inaccurate velocity model, (b) the expected result when using the conventional DSO objective function and (c) the inversion goal.*

Numerical Results

We invert for the velocity and compare the outcomes of the two objectives for a 1D two-layer model. we use a 10% lower velocity as a starting model. As shown in Figure 2, the normalized common image gather (CIG) maintains the amplitude even for the zero offset while the conventional DSO operator does not. To better investigate the difference, we applied the inversion using different smoothing radius, specifically no smoothing, 75 m, 150 m and 300 m. We display the inversion results in Figure 3. Without smoothing the gradient, the inverted model is very oscillatory especially at the reflector depth for the conventional DSO in Figure 3(a). As we increase the smoothing, the results for the conventional DSO improve as shown in Figure 3(b) and 3(c), until the oscillations around the reflector are removed in Figure 3(d). On the contrary, the results for the NDSO are mainly free of oscillations around the reflector and show better convergence as shown in the second row in Figure 3.

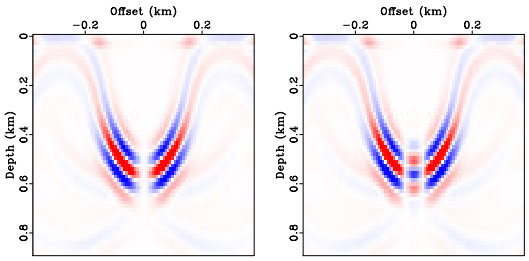

(a) (b)

Figure 2 *CIG for a two-layer model for (a) the conventional penalty operator and (b) for the normalized DSO misfit function*

We also test the inversion using the Marmousi (II) model given in Figure 4(a) for the two objective functions. We used 282 shots separated by 60 m at 45 m depth with 10 Hz peak frequency Ricker wavelet. We use 1132 receivers to record the data placed every 13 m at 45 m depth, as well. We do not apply any smoothing to the gradient in the inversion. The starting model is a linearly increasing 1D model given in Figure 4(b) and the inversion results are shown in Figure 5(a) for the conventional DSO and in Figure 5(b) for the normalized DSO. Their corresponding images are displayed in Figures 6(a), 6(b) and 6(c) . It can be seen that the inversion for the conventional DSO contains more artifacts especially in the left side than the normalized inversion. This is also reflected in the images produced by the inverted

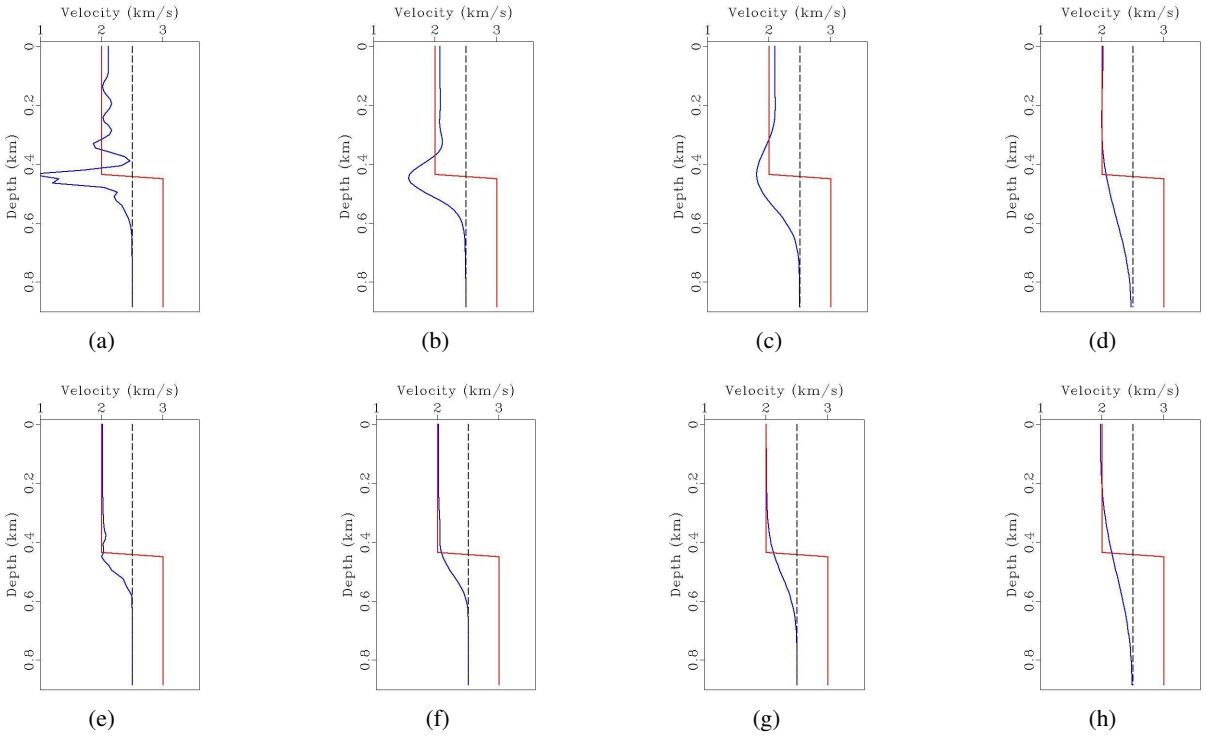

Figure 3 *Inversion results for the conventional DSO in first row and for the normalized DSO in the second row using different smoothing radius. From the left, the smoothing radius is 0, 75 m, 150 m, and 300 m. The red line is the true, the dashed line is the initial and the blue line is the inverted models*

models as indicated by the red arrows. We show CIG in Figure 7 to asses the quality of the images. The initial CIG in Figure 7(a) are not focused due to the velocity error while the final CIG in Figures 7(b) and 7(c) are more focused toward zero subsurface offset indicating the background velocity is correct.

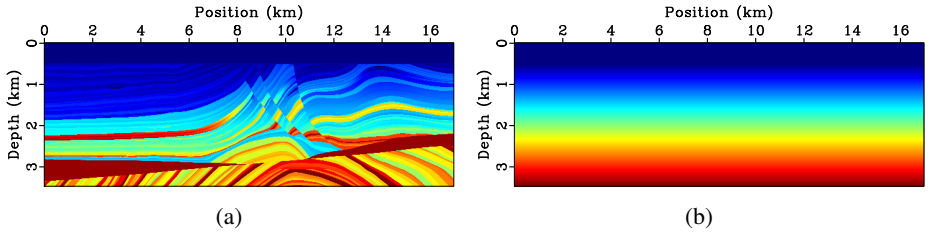

Figure 4 *(a) The Marmoudi II model and (b) is the initial model used in IVA*

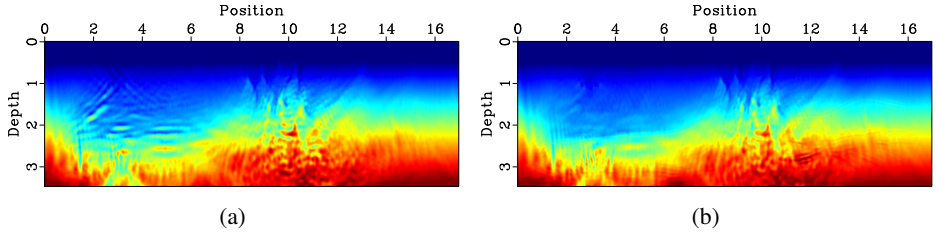

Figure 5 *Inversion results for (a) The conventional DSO objective and (b) the normalized objective*

Conclusions

The conventional DSO objective is only a penalty operator that reduces the energy instead of focussing it toward zero subsurface offset. This leads to undesired behavior and oscillations in the inverted velocity

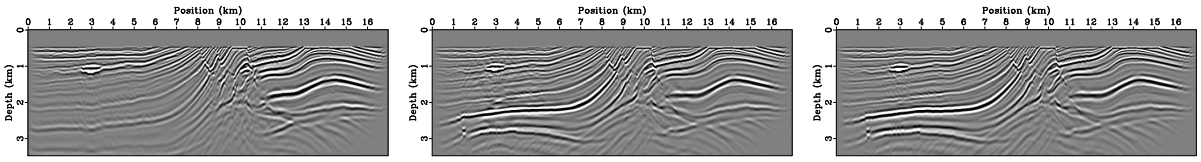

(a) (b) (c)

Figure 6 *Images corresponding to (a) the initial model, (b) the DSO inverted model and (c) the NDSO inverted model.*

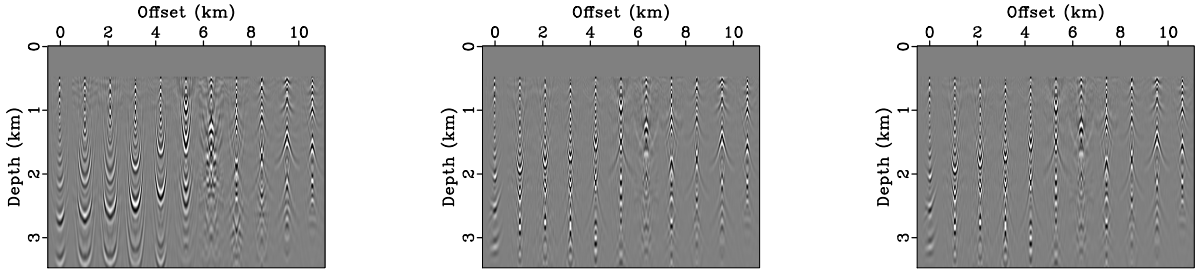

(a) (b) (c)

Figure 7 *CIG corresponding to the images in Figure 6.*

model especially around the reflectors. If sufficient smoothing is applied to the gradient, the oscillations around the reflector can be removed on the expense of reducing resolution. We proposed to normalize the DSO objective to improve the focusing and obtain a steady update. The numerical results showed that the normalized objective improved the update and removed the oscillations even if no smoothing is applied.

References

Chauris, H. and Cocher, E. [2017] From migration to inversion velocity analysis. *Geophysics*, **82**(3), S207–S223.

Lameloise, C.A., Chauris, H. and Noble, M. [2015] Improving the gradient of the image-domain objective function using quantitative migration for a more robust migration velocity analysis. *Geophysical prospecting*, **63**(2), 391–404.

Plessix, R.E. [2006] A review of the adjoint-state method for computing the gradient of a functional with geophysical applications. *Geophysical Journal International*, **167**(2), 495–503.

Rickett, J.E. and Sava, P.C. [2002] Offset and angle-domain common image-point gathers for shot-profile migration. *Geophysics*, **67**(3), 883–889.

Sun, B. and Alkhalifah, T. [2018a] The application of an optimal transport to a preconditioned data matching function for robust waveform inversion. *SEG Technical Program Expanded Abstracts*.

Sun, B. and Alkhalifah, T. [2018b] Automatic wave-equation migration velocity analysis by focusing subsurface virtual sources. *Geophysics*, **83**(2), no. 2, U1–U8.

Sun, B. and Alkhalifah, T. [2018c] Mitigate Cycle Skipping In FWI: A Generalized Instanatenous Travel-Time Approach. *80th EAGE Conference and Exhibition*.

Sun, B. and Alkhalifah, T. [2019] A robust waveform inversion using a global comparison of modeled and observed data. *The Leading Edge*, accepted.

Symes, W.W. [2008] Migration velocity analysis and waveform inversion. *Geophysical prospecting*, **56**(6), 765–790.

Warner, M. and Guasch, L. [2016] Adaptive waveform inversion: Theory. *Geophysics*, **81**(6), R429–R445.